

## MIT Open Access Articles

*Configurations of polymers attached to probes*

The MIT Faculty has made this article openly available. **Please share** how this access benefits you. Your story matters.

**Citation:** Bubis, Roy, Yacov Kantor, and Mehran Kardar. "Configurations of Polymers Attached to Probes." EPL (Europhysics Letters) 88, no. 4 (November 1, 2009): 48001.

**As Published:** <http://dx.doi.org/10.1209/0295-5075/88/48001>

**Publisher:** IOP Publishing

**Persistent URL:** <http://hdl.handle.net/1721.1/88504>

**Version:** Original manuscript: author's manuscript prior to formal peer review

**Terms of use:** Creative Commons Attribution-Noncommercial-Share Alike



# Configurations of polymers attached to probes

ROY BUBIS,<sup>1</sup> YACOV KANTOR<sup>1</sup> and MEHRAN KARDAR<sup>2</sup>

<sup>1</sup> *Raymond and Beverly Sackler School of Physics and Astronomy, Tel Aviv University, Tel Aviv 69978, Israel*

<sup>2</sup> *Department of Physics, Massachusetts Institute of Technology, Cambridge, Massachusetts 02139, USA*

PACS 82.35.Lr – Physical properties of polymers

PACS 64.60.F- – Equilibrium properties near critical points, critical exponents

PACS 36.20.Ey – Conformation (statistics and dynamics)

**Abstract.** - We study polymers attached to spherical (circular) or paraboloidal (parabolic) probes in three (two) dimensions. Both self-avoiding and random walks are examined numerically. The behavior of a polymer of size  $R_0$  attached to the tip of a probe with radius of curvature  $R$ , differs qualitatively for large and small values of the ratio  $s = R_0/R$ . We demonstrate that the scaled compliance (inverse force constant)  $S/R_0^2$ , and scaled mean position of the polymer end-point  $\langle x_\perp \rangle/R$  can be expressed as a function of  $s$ . Scaled compliance is anisotropic, and quite large in the direction parallel to the surface when  $R_0 \sim R$ . The exponent  $\gamma$ , characterizing the number of polymer configurations, crosses over from a value of  $\gamma_1$  – characteristic of a planar boundary – at small  $s$  to one reflecting the overall shape of the probe at large  $s$ . For a spherical probe the crossover is to an unencumbered polymer, while for a parabolic probe we cannot rule out a new exponent.

Recent progress in single molecule manipulation [1] enables direct probing of their properties. Most techniques, from atomic force microscopy [2] and microneedles [3], to optical [4] and magnetic [5] tweezers, have one common feature: the investigated molecule is attached to a probe comparable in size or larger than the molecule itself. Accurate interpretation of the experimental results should thus account for the molecule-probe interactions. Here, we examine some properties – end-point distribution, force-response, and number of configurations – of simple polymers attached to spherical or parabolic probes.

Many properties of long polymer are independent of their microscopic details. For example, the mean squared end-to-end distance of a polymer in a good solvent increases with the number of monomers  $N$  as  $R_0^2 \sim a^2 N^{2\nu}$ , where  $a$  is of order of a monomer size, and the exponent  $\nu$  depends only on the space dimension  $d$  [6]. This universal behavior can be explained by the correspondence between polymers in the  $N \rightarrow \infty$  limit, and thermodynamic systems approaching the critical point of a phase transition [6,7], and is exploited in renormalization group treatments of polymers [8]. Such universality also justifies the use of self-avoiding walks (SAWs) on lattices [9] to model long polymers. While the majority of applications are three-dimensional (3D), studies of two-dimensional (2D) models are important both as a theoretical test bed, and

since the effects of self-avoidance are stronger in lower dimensions: e.g.,  $\nu = 3/4$  in 2D while  $\nu \approx 0.588$  in 3D. (The latter value is closer to  $\nu = 1/2$  which appears in any  $d$  in the absence of self-avoidance.) While self-avoiding walks provide a simple representation of a polymer, (non-self-avoiding) random walks (RWs) [10] may capture some characteristics of polymers in a dense melt [6]. The total number of configurations  $\mathcal{N}_N$  of walks on a lattice scales as  $\mathcal{N}_N \sim \mu^N N^{\gamma-1}$ , where  $\mu$  is a model-dependent connective constant, while the exponent  $\gamma$  is universal and equals to  $43/32$  (1.157) for 2D (3D) SAWs [11], and is 1 for RWs. The universal value of  $\gamma$  can be modified by introducing geometrical restrictions [12] that are present on all length scales: E.g., the number of SAWs attached by one end to an infinite repulsive wall is [13]  $\mathcal{N}_{N,\text{wall}} \sim \mu^N N^{\gamma_1-1}$ , where  $\gamma_1 = 61/64$  (0.679) for 2D [14] (3D [15]) SAWs, and  $\gamma_1 = 1/2$  for RWs [16]. Similar variations occur when a polymer is excluded from a region shaped as a planar wedge in 2D or 3D [14,17], or a cone in 3D [18].

Since real probes usually have rounded end-points, a short polymer (with  $R_0$  smaller than the “rounding”) will behave as if it is in the neighborhood of an infinite flat surface. However, a longer polymer will be influenced by the overall shape of the probe and exhibit crossover to a different asymptotic behavior. In 3D we considered three types of shapes: spheres, semi-infinite cylinders and paraboloids.

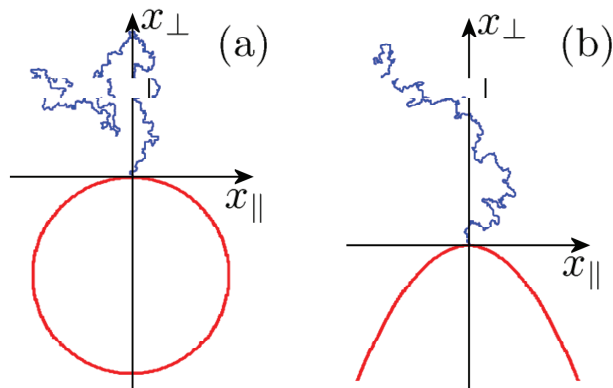


Fig. 1: (Color online) Self-avoiding walks attached to a repulsive (a) circle as in Eq. (1) or (b) parabola as in Eq. (2) (sphere or paraboloid in 3D). The distance  $a_0$  between the upper tip of the probe and the origin of the SAW is equal to a single lattice spacing  $a$  and is not visible on this scale.

We also studied 2D versions of these geometries, since in lower dimension the effects of the probe are stronger. Figure 1 depicts two examples of 2D probes whose surfaces are described by

$$(x_{\perp} + a_0 + R)^2 + x_{\parallel}^2 = R^2, \quad (1)$$

$$x_{\perp} + Cx_{\parallel}^2 = -a_0. \quad (2)$$

Equation (1) defines a circle of radius  $R$ , and Eq. (2) a parabola with curvature  $2C = 1/R$  at its tip. Note that at length scales not exceeding  $R$  the tip of the parabola is similar to the sphere of the same radius. We model the polymer attached to the probe by a RW or SAW which begins at the origin of coordinates, at a small distance  $a_0$  away from the nearest point of the probe surface. The 3D generalization of these surfaces are a sphere and a paraboloid. The axis  $x_{\perp}$  is perpendicular to the surface near the origin, while  $x_{\parallel}$  is parallel to it: In 3D  $x_{\parallel}$  spans the 2D plane parallel to the surface, and  $x_{\parallel}^2$  in Eqs. (1), (2) should be replaced by, say,  $x_2^2 + x_3^2$ . We may expect that very long polymers will see the sphere as a point-like obstacle weakly influencing their behavior, while the cylinder will resemble a semi-infinite excluded line with a larger influence. In either case no length scale should remain visible to long polymers. Paraboloids and parabolas present a slightly more complicated problem: Their width increases as the square-root of the distance from their tip, thus presenting an additional (varying) length scale. The presence of such a sublinearly widening boundary is thought to be insufficient to modify the asymptotic behavior: From the perspective of renormalization group, rescaling of all dimensions by a factor of  $\lambda$  will increase  $C$  by only  $\lambda^{1/2}$ , i.e. make the shape approach a semi-infinite line, and possibly behave as such. Nevertheless, we find that the excluded shape results in interesting effects [19] at finite  $N$ . In this paper we present some results pertaining to circles (spheres) and parabolas (paraboloids) in 2D (3D). Additional properties and geometries will be

described elsewhere [20].

Our numerical simulations were performed on a square (cubic) lattice in 2D (3D) with lattice constant  $a$ . The probe positions were also discretized and thus rough on the same scale. (For  $R \gg a$  we expect discretization effects to be negligible.) We further assume that  $a_0 = a$  does not play a role in the behavior of the polymer. Results were obtained using standard MC procedures: the samples of SAWs were generated using dimerization [21] and pivoting [22] algorithms, while RWs were either generated randomly, or the end-point distributions were found by solving the diffusion equation with the probe surface as an absorbing boundary.

In the absence of an external force the probability distribution of the end-to-end vector is the ratio between the number of spatial configurations  $\mathcal{N}_N(\vec{r})$  terminating at the position  $\vec{r}$  and the total number of different configurations  $\mathcal{N}_N$  of the walk:  $P(\vec{r}) = \mathcal{N}_N(\vec{r})/\mathcal{N}_N$ . For the probes depicted in Fig. 1 the mean position  $\langle x_{\perp} \rangle$  of the endpoint of the polymer will be along the  $x_{\perp}$  axis. When the lattice constant is significantly shorter than all other scales of the problem, the probability density  $P(\vec{r})/a^d$  of the end-point position no longer explicitly depends on  $a$  and  $N$ , and only depends on the polymer size  $R_0$  and the characteristic length  $R$  of the probe [6]. Consequently,  $\langle x_{\perp} \rangle$  which has dimensions of length must behave as  $R\Phi(R_0/R)$ , where  $\Phi$  is a dimensionless function of the variable  $s = R_0/R$ . (This argument applies to both spheres and paraboloids. However, the function  $\Phi$  will be different in each case.) Figure 2 depicts  $\Phi(s)$  calculated for SAWs near a sphere and a paraboloid in 3D. The results for several values of  $R$  and a large range of  $N$  nicely collapse, confirming our scaling assumption. For  $s \ll 1$  the polymer does not “feel” the curvature of the surface, and the result should be independent of  $R$ . This requires that  $\Phi(s) \sim s$  for small  $s$ . Indeed, the insets depict the expected linear small- $s$  behavior. Moreover, the slopes obtained for the sphere and parabola coincide, because in this range they are independent of the shape of the probe. (The factor 2 in the relation  $C = 1/2R$  does not influence these graphs because both axes include  $C$  as a prefactor.) Similar small- $s$  behavior was obtained for SAWs in 2D and for RWs in both 2D and 3D.

For large  $s$ , the behavior of  $\Phi(s)$  depends on the space dimension, and the type of walk used to model the polymer, as well as on the type of the probe. The behavior near a sphere is the simplest: For SAWs the scaling function in top Fig. 2 approaches a constant, i.e.  $\langle x_{\perp} \rangle$  stops increasing. We find a similar behavior for a RW [20]. Both cases are consistent with the fact that the mean distance between the origin and the endpoint of a SAW or RW that starts near an excluded point in 3D is finite [23]. The situation is different in 2D: We find [20] that the presence of the excluded circle causes a logarithmic divergence of  $\Phi$  for RWs, similar to the behavior in the presence of an excluded point [23, 24] (since the RW keeps returning to the origin). The behavior of 2D SAWs in the presence of

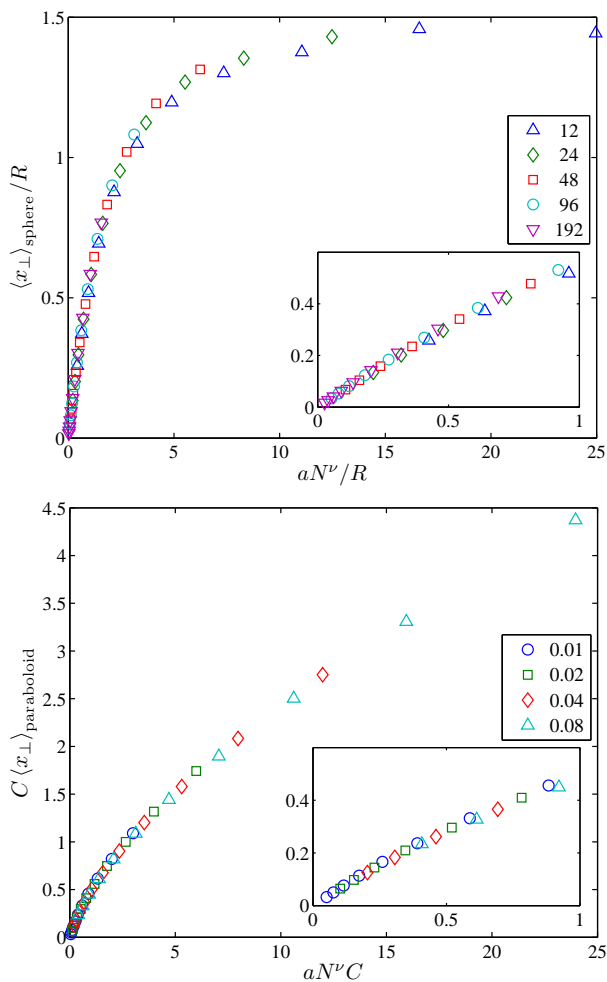


Fig. 2: (Color online) The scaling function for the mean end-point position of 3D SAW with  $N$  ranging from 16 to 16384 for a sphere (top panel) with  $R$  from 12 to 192 lattice constants (see legend); and a paraboloid (bottom panel) with  $C$  between 0.01 and 0.08 inverse lattice constants (see legend). The insets show the behavior for small values of (top)  $aN^{\nu}/R$  and (bottom)  $CaN^{\nu}$ . Error bars are smaller than the size of the symbols.

an excluded point is less clear, and arguments for both diverging  $\Phi$  [25, 26] and convergence to a constant [27] have been advanced. Our results [20] were unable to distinguish between convergence to a constant and a slower-than-logarithmic divergence.

The behavior of a polymer near a parabola or paraboloid deserves more careful examination. Even the presence of a semi-infinite excluded line has severe effects on the mean position of the end-point. In 2D that point moves away from the starting point as  $aN^{\nu}$  for both RWs and SAWs. Clearly  $\langle x_{\perp} \rangle \sim R_0$  (i.e.  $\Phi(s) \sim s$ ) is as far away as the end-point is likely to go and therefore, unsurprisingly, we get the same result for a parabola [20]. The separation of the end-point in 3D is more striking: For the semi-infinite line the mean position of the end-point of a RW moves away a distance  $aN^{1/2}/\ln N$  [23]. This result is barely distinguishable from the maximal conceivable separation

$aN^{1/2}$  and our results for the parabolic probe closely follow this prediction. More interestingly, the mean position of an end-point of SAWs attached to the tip of a semi-infinite line in 3D is reported to increase as  $aN^{\sigma}$  with  $\sigma \approx 0.4$  [23, 28, 29]. If we assume that this result is also valid for a paraboloid we must have  $\Phi(s) \sim s^{\alpha}$ , with  $\alpha = \sigma/\nu$ . The high- $s$  end of the data depicted in the Fig. 2(b) can be fitted with  $\alpha \approx 0.71$  which is close to the value 0.68 obtained in the simulations of polymers near a semi-infinite line [23].

Force-displacement characteristics are quite relevant to experiments. The necessary information to obtain such relations is contained in the details of the end-point probability distribution  $P(\vec{r})$ . This distribution plays the role of the Boltzmann weight in this ensemble, since the energy is constant and each configuration has the same probability. When a force  $\vec{f}$  is applied to the end-point of the polymer, the probability distribution is shifted by a corresponding Boltzmann weight, such that the mean position of the end-point of the walk is obtained by

$$\langle \vec{r} \rangle_{\vec{f}} = \frac{\int \vec{r} P(\vec{r}) e^{\vec{f} \cdot \vec{r}/k_B T} d^d \vec{r}}{\int P(\vec{r}) e^{\vec{f} \cdot \vec{r}/k_B T} d^d \vec{r}}. \quad (3)$$

The probability  $P(\vec{r})$  in the presence of a repulsive probe is not isotropic, and therefore the position of the end-point is not necessarily directed along the force. However, since the system is symmetric with respect to  $x_{\perp}$ , by expanding Eq. (3) to the first order in  $\vec{f} \cdot \vec{r}/k_B T$ , we find

$$\langle \vec{r} \rangle_{\vec{f}} = (\langle x_{\perp} \rangle + S_{\perp} f_{\perp}) \hat{\mathbf{x}}_{\perp} + S_{\parallel} f_{\parallel} \hat{\mathbf{x}}_{\parallel}, \quad (4)$$

where  $\langle \rangle$  without the subscript  $\vec{f}$  denotes the averages in the *absence* of external force, and the compliances  $S_{\perp, \parallel}$  (inverse force constants) are given by the variance of the end-point position with zero force, i.e.  $S_{\perp} = \text{var}(x_{\perp})/k_B T$  and  $S_{\parallel} = \text{var}(x_{\parallel})/k_B T$ . Such linear response is only valid for small forces, i.e. when  $f \ll k_B T/R_0$ . This requirement corresponds to force-induced displacements that are smaller than  $R_0$ . The large force regime is not considered in this work, but may be treatable by using the concept of blobs [6]. Should the experimental setup make it necessary, these results could be extended to probes attached to both ends of the polymer.

Since the variance of the position of end-point has dimensions of squared length, it can be expressed as  $R_0^2 \Phi_{\perp, \parallel}(R_0/R)$ . Consequently, the ratio between the variance and  $R_0^2$  should only depend on  $s = R_0/R$ , and not separately on  $R$  or  $N$ . The scaling functions  $\Phi_{\perp, \parallel}(s)$  will be different for spheres and paraboloids and will depend on space dimension. Figure 3 demonstrates nice collapse of data obtained for different values of  $R$  or  $C$  and a large range of  $N$ . For small  $s$  we note that all the curves approach a constant indicating that, as expected, the compliance is proportional to  $R_0^2$ . There are no differences between the spherical and paraboloidal probes in this limit since the polymer behaves as if it is near an infinite plane.

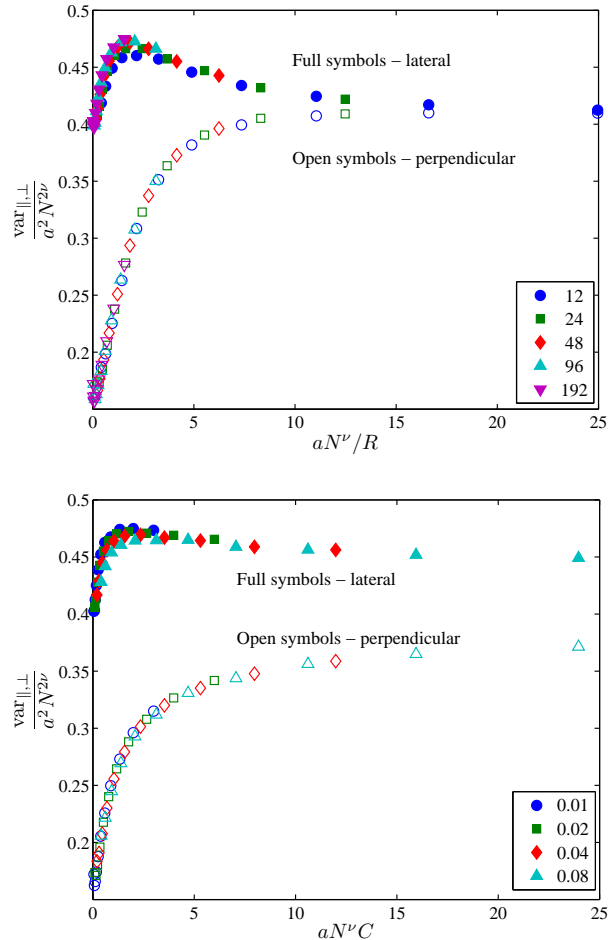


Fig. 3: (Color online) The scaling function for the linear response to force of a three-dimensional SAW near a sphere (top panel) with  $R$  from 12 to 192 lattice constants (see legend) and near a paraboloid (bottom panel) with  $C$  between 0.01 and 0.08 inverse lattice constants (see legend), for  $N$  ranging from 16 to 16384. Open (full) symbols indicate response to a perpendicular (lateral) force. Error bars are smaller than the size of the symbols.

We note a significant difference between the lateral and perpendicular compliances - the former is almost thrice the latter, i.e. it is easier to displace the end-point of the polymer parallel to the plane. For large values of  $s$  the differences between the two compliances disappear in the case of a sphere, since it no longer influences the polymer. However, quantitative differences persist for the paraboloid, since the presence of the probe is strongly felt for any  $R_0$  as already noted in measurements of the mean position of the end-point.

Both for spheres and paraboloids,  $\Phi$  interpolates between the expected small- $s$  and the very-large- $s$  limits. Less expected is the non-monotonic behavior of  $\Phi_{||}(s)$ : the function has a maximum for  $s$  of order unity, i.e. when the size of the polymer becomes comparable with the typical length-scale of the probe. This feature persists for

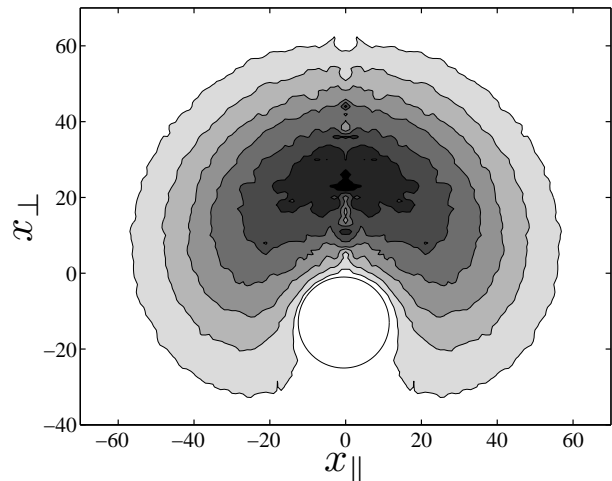


Fig. 4: Probability distribution of the endpoint of a 3D SAW with  $N = 512$  near a sphere of radius  $R = 12a$ . The contour plot shows a cut through  $x_3 = 0$ . Darker color indicates higher probability density. Contour lines are equally spaced on linear scale. Ruggedness of the lines is a consequence of discreteness of the lattice.

SAWs in 2D and is equally pronounced for RWs both in 2D and in 3D [20]. It should be noted that for any value of  $R_0$ , the variance of the position of the end point is of the order of  $R_0^2$ . That variance (and consequently, the compliance constant) remains a monotonically increasing function of  $R_0$ . However, the *prefactor* for lateral fluctuations becomes somewhat larger when  $R_0$  is of the same order as the probe. To understand this effect we examine the probability density of the end-point of a SAW attached to a sphere. Figure 4 depicts a cut through the three dimensional probability for  $x_3 = 0$ . This contour plot presents a case when the size of the polymer is comparable with the radius of the sphere. The strong distortion caused by the sphere (the probability density appears to “hug” the sphere) enhances the probabilities at large values of  $|x_{||}|$  at the expense of areas close to  $x_{||} = 0$ , partly explaining the larger variance.

Interesting insights into the statistical mechanics of polymers can be obtained from a direct study of their free energy, which is proportional to the logarithm of the partition function  $Z$ . The configuration part of  $Z$  is simply the number of possible states of the polymer in the presence of the probe; its dependence on  $N$  exhibits interesting crossovers. We will use the sphere to demonstrate the general trends. While the exponentially increasing part of the number of states ( $\mu^N$ ) is unaffected by the presence of the probes, the power law dependence of the number of states on  $N$  is modified. We know that for  $R_0 \ll R$  the sphere’s surface is indistinguishable from an infinite plane, and therefore  $\mathcal{N}_{N,\text{sphere}} \sim \mu^N N^{\gamma_1-1}$ , as expected for a walk near a wall [14–16]. Consequently,  $\mathcal{N}_{N,\text{sphere}}/\mathcal{N}_N \sim N^{\gamma_1-\gamma}$ . On the other hand, when  $R_0 \gg R$ , the behavior is expected to match that of a walk near an excluded point.

Since the ratio between  $\mathcal{N}_N$  and the number of walks with excluded point remains finite, we expect  $\mathcal{N}_{N,\text{sphere}}/\mathcal{N}_N$  to approach a constant. The crossover between two behaviors appears when  $R_0 \sim R$ , and an appropriate scaling assumption is

$$\frac{\mathcal{N}_{N,\text{sphere}}}{\mathcal{N}_N} = \left(\frac{R}{a}\right)^{\frac{\gamma_1 - \gamma}{\nu}} \Psi\left(\frac{aN^\nu}{R}\right). \quad (5)$$

In the limit of short walks we expect  $\Psi(s \rightarrow 0) \sim s^{(\gamma_1 - \gamma)/\nu}$ , eliminating the dependence on  $R$ , while for  $s \rightarrow \infty$  the function should approach a constant. We verified this scaling behavior numerically for both SAWs and RWs in 3D and 2D, by examining spheres (circles) with several radii and a wide range of  $N$ . For small  $s$  we obtained power law dependencies differing only by few percent from the known values. E.g., for 3D SAWs near a sphere we found  $(\gamma_1 - \gamma)/\nu \approx -0.81$ , while the expected value is  $-0.78$  [6, 11, 15]. We obtained reasonable data collapse for all cases [20] confirming the scaling form in Eq. (5). (The 2D case of RWs is slightly different since the fraction of walks not returning to the vicinity of the origin decreases as  $1/\ln N$ , thus introducing a slight correction.)

For a semi-infinite cylinder or rectangle of width  $2W$  one can modify Eq. (5) to read

$$\frac{\mathcal{N}_{N,W}}{\mathcal{N}_N} = \left(\frac{W}{a}\right)^{\frac{\gamma_1 - \gamma}{\nu}} \Psi\left(\frac{aN^\nu}{W}\right). \quad (6)$$

As in the case is a sphere, for small  $s$  we expect  $\Psi \sim s^{(\gamma_1 - \gamma)/\nu}$ , eliminating the dependence on  $W$ . In the limit of large  $N$  we expect the behavior near a semi-infinite line. The latter has been extensively studied: In general, the number of states of a walk attached to the tip of a semi-infinite line increases as  $\mu^N N^{\gamma_{\text{line}} - 1}$ . In 3D the presence of the semi-infinite line does not influence the number of states, i.e.  $\gamma_{\text{line}}$  for SAWs coincides with  $\gamma$  of unrestricted walks [29]. (For RWs there is a logarithmic correction [23].) In 2D the presence of the line has a more significant effect and  $\gamma_{\text{line}} = 76/64$  for SAWs [14, 17], and  $\gamma_{\text{line}} = 3/4$  for a RW [23]. Consequently, for a rectangular/cylindrical probe at large  $s$  we must assume that  $\Psi \sim s^{(\gamma_{\text{line}} - \gamma)/\nu}$ , leading to the large- $N$  dependence

$$\frac{\mathcal{N}_{N,W}}{\mathcal{N}_N} \approx \left(\frac{W}{a}\right)^{\frac{\gamma_1 - \gamma_{\text{line}}}{\nu}} N^{\gamma_{\text{line}} - \gamma}. \quad (7)$$

Our numerical results confirmed this type of behavior for RWs and SAWs, both for rectangles in 2D and for cylinders in 3D [20].

The number of states of a polymer near a parabola (paraboloid) presents a more challenging problem. At length scales shorter than the curvature  $R = 1/2C$  of the tip we find results indistinguishable from the behavior near a sphere. However, for large  $N$  curvature is no longer the relevant length scale since the parabola keeps widening. At every length scale we may think of the parabola

Table 1: Exponent  $\gamma_{\text{par}}$  near a parabolic probe: numerical estimates *vs.* lower and upper bounds

	2D parabola			3D paraboloid		
	num.	lower	upper	num.	lower	upper
RW	0.70	0.63	0.75	0.82	0.75	1.00
SAW	1.14	1.07	1.19	0.99	0.92	1.16

(paraboloid) as bounded from inside by a cylinder of width  $W = a$  and from outside by a cylinder of width  $W = \sqrt{aN^\nu/C}$ . These two geometries provide upper and lower bounds on the number of states of the polymer near a parabola (paraboloid)  $\mathcal{N}_{N,\text{par}}$ . If  $\mathcal{N}_{N,\text{par}}/\mathcal{N}_N \sim N^{\gamma_{\text{par}} - \gamma}$  then  $(\gamma_{\text{line}} + \gamma_1)/2 \leq \gamma_{\text{par}} \leq \gamma_{\text{line}}$ . Our numerical studies of  $\mathcal{N}_{N,\text{par}}$  produced rather low quality data collapse, and Table 1 presents our estimates for the exponent  $\gamma_{\text{par}}$ , for RW/SAW in 2D/3D. The few percent statistical errors of each of those estimates is probably smaller than the possible systematic error. All our results were within the exact bound on the exponent also presented in Table 1. (The bounds were calculated from the values of  $\gamma$  that are either known exactly or with high numerical accuracy, and therefore the uncertainties are smaller than the last included digit.) Our range of lengths was insufficient to ascertain if these are true power laws, or crossover effects.

In summary, we have demonstrated the strong influence of repulsive probes on the properties of a polymer. Our results regarding the force constants demonstrate significant differences between lateral and perpendicular responses, and an unexpected non-monotonic dependence of the coefficient of the former. In single molecule experiments the applied forces range between 0.1pN and 1000pN, and the weak deformation regime is usually at the low end of this range. Most of the measurements involve perpendicular forces, although measurements of lateral forces also exist [30]. As the experimental techniques become more refined our results will become more relevant, making it worthwhile to examine additional geometries. Further study is needed to understand the behavior of the number of states near a parabola (or paraboloid) to distinguish between possible crossover effects and new exponents.

\*\*\*

This work was supported by the Israel Science Foundation under Grant No. 99/08 (Y.K.) and by the National Science Foundation under Grant No. DMR-08-03315 (M.K.).

## REFERENCES

- [1] BUSTAMANTE C., BRYANT Z. and SMITH S. B., *Nature*, **421** (2003) 423; KELLERMAYER M. S., *Physiol. Meas.*, **26** (2005) R119; NEUMAN K., LIONNET T. and ALLEMAND J.-F., *Ann. Rev. Mater. Res.*, **37** (2007) 33; DENIZ A. A.,

- MUKHOPADHYAY S. and LEMKE E. A., *J. R. Soc. Interface*, **5** (2005) 15.
- [2] FISHER T. E., MARSZALEK P. E., OBERHAUSER A. F., CARRION-VAZQUEZ M. and FERNANDEZ J. M., *J. Physiol.*, **520** (1999) 5.
- [3] KISHINO A. and YANAGIDA T., *Nature*, **334** (1988) 74.
- [4] HORMEÑO S. and ARIAS-GONZALEZ J. R., *Biol. Cell*, **98** (2006) 679.
- [5] GOSSE C. and CROQUETTE V., *Biophys. J.*, **82** (2002) 3314.
- [6] DE GENNES P.-J., *Scaling Concepts in Polymer Physics* (Cornell University Press, Ithaca, New York) 1979.
- [7] KARDAR M., *Statistical Physics of Fields* (Cambridge University Press) 2007.
- [8] SCHÄFER L., *Excluded Volume Effects in Polymer Solutions* (Springer, Berlin) 1999.
- [9] LI B., MADRAS N. and SOKAL A. D., *J. Stat. Phys.*, **80** (1995) 661.
- [10] HUGHES B. D., *Random Walks and Random Environments*, Vol. **1** (Clarendon Press, Oxford) 1995; RUDNICK J. and GASPARI G., *Elements of the Random Walk* (Cambridge University Press) 2004.
- [11] GRASSBERGER P., SUTTER P. and SCHÄFER L., *J. Phys. A: Math. Gen.*, **30** (1997) 7039; CARACCILO S., CAUSO M. S. and PELISSETTO A., *Phys. Rev. E*, **57** (1998) R1215; NIENHUIS B., *Phys. Rev. Lett.*, **49** (1982) 1062.
- [12] BINDER K., in *Phase Transitions and Critical Phenomena*, Vol. **8**, edited by DOMB C. and LEBOWITZ J. L. (Academic Press, London) 1983, p. 1.
- [13] WHITTINGTON S. G., *J. Chem. Phys.*, **63** (1975) 779.
- [14] CARDY J. L., *Nucl. Phys. B*, **240** (1984) 514.
- [15] GRASSBERGER P., *J. Phys. A: Math. Gen.*, **38** (2005) 323.
- [16] DE'BELL K. and LOOKMAN T., *Rev. Mod. Phys.*, **65** (87) 1993.
- [17] CARDY J. L., *J. Phys. A: Math. Gen.*, **16** (1983) 3617; CARDY J. L. and REDNER S., *ibid.*, **17** (1984) L933; GUTTMANN A. J. and TORRIE G. M., *ibid.*, **17** (1984) 3539.
- [18] SLUTSKY M., ZANDI R., KANTOR Y. and KARDAR M., *Phys. Rev. Lett.*, **94** (2005) 198303.
- [19] PESCHEL I., TURBAN L. and IGLÓI F., *J. Phys. A: Math. Gen.*, **24** (1991) 1229.
- [20] BUBIS R., KANTOR Y. and KARDAR M., to be published.
- [21] SUZUKI K., *Bull. Chem. Soc. Jpn.*, **41** (1968) 538; ALEXANDROWICZ Z., *J. Chem. Phys.*, **51** (1969) 561.
- [22] LAL M., *Molec. Phys.*, **17** (1969) 57; MADRAS N. and SOKAL A. D., *J. Stat. Phys.*, **50** (1988) 109.
- [23] CONSIDINE D. and REDNER S., *J. Phys. A: Math. Gen.*, **22** (1989) 1621.
- [24] WEISS G. H., *J. Math. Phys.*, **22** (1981) 562.
- [25] GRASSBERGER P., *Phys. Lett. A*, **89** (1982) 381; MEIROVITCH H., *J. Chem. Phys.*, **79** (1983) 502; LIM H. A. and MEIROVITCH H., *Phys. Rev. A*, **39** (1989) 4176; BURNETTE D. E. and LIM H. A., *J. Phys. A: Math. Gen.*, **22** (1989) 3059.
- [26] REDNER S. and PRIVMAN V., *J. Phys. A: Math. Gen.*, **20** (1987) L857.
- [27] EISENBERG E. and BARAM A., *J. Phys. A: Math. Gen.*, **36** (2003) L121.
- [28] VANDERZANDE C., *J. Phys. A: Math. Gen.*, **23** (1990) 563; GRASSBERGER P., *J. Phys. A: Math. Gen.*, **26** (1993) 2769; CARACCILO S., CAUSO M. S. and PELISSETTO A., *J. Phys. A: Math. Gen.*, **30** (1997) 4939.
- [29] CARACCILO S., FERRARO G. and PELISSETTO A., *J. Phys. A: Math. Gen.*, **24** (1991) 3625;
- [30] BULGAREVICH D. S., MITSUI K. and ARAKAWA H., *J. Phys. Conf. Ser.*, **61** (2007) 170.